CORA Cork Open Research Archive
Cartlann Taighde Oscailte Chorcaí

Title	Development of a facile block copolymer method for creating hard mask patterns integrated into semiconductor manufacturing
Authors	Ghoshal, Tandra;Shaw, Matthew T.;Holmes, Justin D.;Morris, Michael A.
Publication date	2016-07-26
Original Citation	Ghoshal, T., Shaw, M. T., Holmes, J. D. and Morris, M. A. (2016) 'Development of a facile block copolymer method for creating hard mask patterns integrated into semiconductor manufacturing', Nano Research, 9(10), pp. 3116-3128. doi: 10.1007/s12274-016-1194-7
Type of publication	Article (peer-reviewed)
Link to publisher's version	10.1007/s12274-016-1194-7
Rights	© Tsinghua University Press and Springer-Verlag Berlin Heidelberg 2016. This is a post-peer-review, pre-copyedit version of an article published in Nano Research. The final authenticated version is available online at: http://dx.doi.org/10.1007/s12274-016-1194-7
Download date	2026-11-15 18:17:51
Item downloaded from	https://hdl.handle.net/10468/6789

UCC
University College Cork, Ireland
Coláiste na hOllscoile Corcaigh

Development of a Facile Block Copolymer Method for Creating Hard Mask Patterns Integrated into Semiconductor Manufacturing

Tandra Ghoshal,[1,2*] Matthew T. Shaw,[3] Justin D. Holmes,[1,2] Michael A. Morris[2*]

[1]Department of Chemistry and Tyndall National Institute, University College Cork, Cork, Ireland

[2]AMBER, Centre for Research on Adaptive Nanostructures and Nanodevices (CRANN), Trinity College Dublin, Dublin, Ireland.

[3]Intel Ireland Ltd., Collinstown Industrial Estate, Co. Kildare, Ireland

[*] Corresponding Author:

Prof. Michael A. Morris

Tel: +353 1 896 3089

Fax: +353 1 896 3089

E-mail: morrism2@tcd.ie

And

Tandra Ghoshal

Tel: + 353 21 490 2911

Fax: +353 21 427 4097

E-mail: g_tandra@yahoo.co.in

ABSTRACT: The aim here is the development of a facile process to create patterns of inorganic oxides and metals on a substrate that can act as hard masks within a lithographic process. These materials should have high etch contrast (to silicon) and so allow high aspect, high fidelity pattern transfer whilst being readily integrate-able in modern semiconductor fabrication (FAB friendly). Here, we show that ultra-small dimension hard masks can be used to develop large areas of densely packed vertically and horizontally orientated Si nanowire arrays. The inorganic and metal hard masks (Ni, NiO and ZnO) of different morphologies and dimensions were formed using microphase separated polystyrene-b-poly(ethylene oxide) (PS-b-PEO) block copolymer (BCP) thin films though the variation of BCP molecular weight and the annealing conditions such as temperature, solvent/s *etc.*. The self-assembled polymer patterns were solvent processed and metal ions included into chosen domains via a selective inclusion method and subsequent inorganic oxide nanopatterns were developed using standard techniques. It is shown by high resolution transmission electron microscopy studies that high aspect pattern transfer could be affected by standard plasma etch techniques. The masking ability of the different materials was compared in order to create the highest quality uniform and smooth sidewall profile of the Si nanowire arrays. Notably, good performance of metal mask was seen and this could impact the use of these materials at small dimension where conventional methods are severely limited.

KEYWORDS: Block Copolymer, self-assembly, hard mask, silicon, nanowires

1. Introduction

Vertical and horizontal orientated (to a substrate surface plane) Silicon (Si) nanofeatures have important applications in nanoelectronics, photonics, sensors and biointerfaces.[1-3] In these applications, there is a clear need to fabricate nano-architectures with morphological/structural regularity, i.e. strict control of their arrangement, size, shape as well as crystallographic orientation. Block copolymer (BCP) based lithographies have high potential as an alternative to conventional photolithography.[4-5] Here, structurally defined nanopatterns are formed due to microphase separation and, with correct processing techniques, can form a series of nanoscale, structural arrangements close in quality to those formed by top-down lithographic processes.[6-10] The advantages of BCP methods compared to other lithographic techniques, such as ion-beam or electron-beam lithography, is that they can provide high throughput capability at relatively low cost.

However, organic BCP systems have severe pattern transfer limitations as there is limited etch contrast between two blocks and high aspect ratio, high quality features are challenging to form. An example is the polystyrene-b-polymethylmethacrylate system where high aspect features are difficult to achieve using conventional plasma etch techniques.[11-12] Various methods have been used to enhance etch contrast and we have been central in developing simple solution mediated metal ion insertion to produce inorganic patterns from the BCP arrangement that can act as 'hard' masks to allow facile and efficient, high aspect ratio pattern transfer.[13-17] However, most of our work has been around iron systems and this material is not compatible with high volume silicon device manufacture.

A significant issue for the fabrication of BCP derived nanostructures is controlling the orientation (i.e. vertical or parallel to the substrate surface) of the microdomains by definition of the BCP molecular weight, composition and in particular, interfacial interactions between the film and the substrate.[18-19] Many strategies have been investigated to manipulate

interfacial interactions, to define orientation (as well as lateral alignment) of the microdomains including external fields (magnetic, electrical), thermal gradients during annealing, mechanical effects (rubbing) and pre-defined substrate topographical and chemical patterning.[20-23] The cylindrical phase BCP systems appear to be more easily controlled than lamellar arrangements since interfacial energy control is less demanding.[24] We, amongst other workers, have shown that solvent annealing is an attractive method controlling orientation since highly ordered arrangements can be rapidly achieved[25-26] while the microdomain orientation is dictated by a complex interplay of surface energies, polymer-solvent interactions, and the commensurability between the film thickness.[27] However, the pattern transfer of the cylindrical phase system is extremely challenging because of the distribution of one block in a matrix of the other and the small diameter of the cylinders which results in poor etch selectivity and shape control.[28-30]

The pattern transfer performance is generally judged by etch rate, selectivity, uniformity, directionality, etched surface quality and reproducibility. Dielectric materials (SiO_2, Al_2O_3 and Si_3N_4 etc.), various metal oxides and metals have been used as 'hard' etch masks [31-34] because of their etch resistance relative to silicon. However, they require complex, multi-step pattern transfer processes from the pre-fabricated patterns. [31] Metals (Cr, Ni), are somewhat limited in use, particularly for small feature sizes, as they are usually patterned by a lift-off technique but this can result significant distortion of the patterns and metal etching can present challenges.[32-35] It should be recognized that advances in etch mask materials coupled to development of facile process at lower cost, could be important for the economics of the semiconductor and other patterning industries.[36-37] Thus, our work on pattern transfer using iron oxide masks might have real relevance since it combines simple, controlled self-assembly with an *'insitu'* hard mask technique.[13-15-17]

Herein, Our previous work is extended towards a detailed assessment of the applicability of different types of compatible etch masks (notably including metals) for the fabrication of high aspect ratio vertically and horizontally aligned Si nanopatterns. As well as extending the materials range, we have carried out extensive high resolution TEM to probe the pattern transferred features in detail. Moreover, the size, shape and areal density can be controlled. It is shown that the ability of various inorganic and metal etch masks to create good sidewall profile, uniform Si nanorods and nanowires through a plasma based pattern transfer process. This fabrication technique therefore mitigates the etch limitation issues comprises with current lithographic processes with high throughput at lower lost. The limitations of the methodology are discussed.

2. Experimental

Preparation of hard masks nanopatterns by block copolymers: Three asymmetric cylinder forming PS-b-PEO diblock copolymers, M_n = 42-11.5 kg mol^{-1}, M_w/M_n = 1.07; M_n = 32-11 kg mol^{-1}, M_w/M_n = 1.06; M_n = 16-5 kg mol^{-1}, M_w/M_n = 1.04 (where, M_n is the number-average molecular weight and M_w is the weight-average molecular weight) were purchased from Polymer Source (Inc., Canada). These were chosen to give a range of feature sizes of 10 nm to 25 nm so that we could examine the efficacy of pattern transfer over a range of feature sizes. Single crystal B doped P type silicon (100) wafers (thickness 650 mm, resistivity 6–14 ohm cm) with a native oxide layer were used as a substrate. Substrates were cleaned by ultrasonication in acetone and toluene for 30 minutes in each solvent and dried under nitrogen. PS-b-PEO was dissolved in toluene to yield 1 wt% polymer solution and aged for 12 h at room temperature. The PS-b-PEO thin film was formed by spin coating the polymer solution (3000 rpm for 30 s). The films were exposed to different solvents vapor (toluene) or a combination of solvents (toluene-water) vapors which were taken in glass viol/s placed at the bottom of a closed vessel at a temperature 50^0C or 60^0C to induce necessary chain

mobility and allow microphase separation to occur to create hole and line/space patterns. Partial etching and domain modification of PEO was carried out by ultrasonication of the films for different time period in anhydrous alcohol at room temperature. After the desired time, the films were taken out from alcohol and dried immediately. For the fabrication of hard masks nanopatterns, the inorganic salt precursor was dissolved in ethanol and spin-coated onto the activated film. UV/Ozone treatment was used to oxidize the precursor and remove polymer. Nickel nitrate hexahydrate ($Ni(NO_3)_3,6H_2O$) and zinc nitrate hexahydrate ($Zn(NO_3)_3,6H_2O$) were used as precursors. Nickel oxide nanopatterns were reduced under Ar/H_2 atmosphere at a temperature of 800^0C for 4 h to generate nickel metal nanostructures.

Pattern transfer using ICP etch: These horizontal and vertical oriented oxides and metal nanowire arrays were used as hard mask for pattern transfer to the substrate using an STS, Advanced Oxide Etch (AOE) inductively coupled plasma (ICP) etcher as previously reported.[15] Scheme 1 (I) and (II) represents the fabrication steps for vertical and horizontal aligned Si nanowires arrays. The system has two different RF generators, the first, generates and controls the plasma density whilst the other control ion energy. A two stage etching process was used to, firstly, etch the native silica layer and, secondly, the silicon substrate. During etching, the sample is thermally bonded to a cooled chuck (10^0C) with a pressure 9.5 Torr. For the oxide layer etch, the process parameters were optimised to a C_4F_8/H_2 gas mixture (21 sccm/30 sccm) using an ICP coil power of 800 W and a Reactive Ion Etching (RIE) power of 80 W. The silica etch time was kept constant (5 sec) for all the samples. For Si pillar fabrication, the process used a controlled gas mixture of C_4F_8/SF_6 at flow rates of 90 sccm/30 sccm respectively and the ICP and RIE power were set to 600 W and 15 W respectively at a chamber pressure of 15 mTorr.

Characterizations: Surface morphologies were imaged by scanning probe microscopy (SPM, Park systems, XE-100) in tapping mode and scanning electron microscopy (SEM, FEI

Company, FEG Quanta 6700 and Zeiss Ultra Plus). The film thicknesses were measured by optical ellipsometer (Woolam M2000) and electron microscopy. Samples were prepared for TEM cross sectional imaging with an FEI Helios Nanolab 600i system containing a high resolution Elstar™ Schottky field-emission SEM and a Sidewinder FIB column and were further imaged by transmission electron microscopy (TEM, JEOL 2100 and TEM, FEI Titan). X-Ray photoelectron spectroscopy (XPS) experiments were conducted on a Thermo K-alpha machine with Al K_α X-ray source operating at 72 W.

3. Results and Discussion

3.1. BCP microphase separation: dimensional, morphological and orientation control. We firstly briefly review the effect of solvents and annealing temperature on the morphology and orientation of different molecular weight cylindrical PS-PEO patterns where PEO is the minority cylinder forming block. The dimensional control over the self-assembled block copolymer nanopatterns was achieved by different molecular weight PS-PEO systems and the corresponding compositions of the constituent blocks represented as S1 (42k-11.5k), S2 (32k-11k) and S3 (16k-5k). The coated films were annealed at a temperature 50^0 C or 60^0 C either in toluene or in toluene/water mixed solvents vapours to induce phase separation and control the orientation of the cylindrical domains. Conditions were highly dependent on the block compositions. Fig. 1 shows the representative tapping mode AFM images of the PS-b-PEO systems after the solvent vapour exposure and indicates ordered arrangements over large areas with no indication of de-wetting. Well-ordered regular dot patterns were realized for S1 and S3 (Figs. 1a and c) when exposed to toluene/water vapour and S2 (Fig. 1b) in toluene at a temperature 50^0 C for 1h. The solvent/s chosen for solvent annealing depending on the molecular weight and weight fraction of PS (f_{PS}) of the systems.[17] A cylindrical reorientation to horizontally aligned fingerprint patterns was noticed for S1 when annealed under toluene vapour at a temperature of 60^0 C (Fig. 1d). The films are of regular thicknesses

of 40 nm, 25 nm and 35 nm for S1, S2 and S3 respectively irrespective of the cylinder orientation (Table 1). No large scale surface roughness or thickness undulation was observed. The corresponding average centre to centre distances between adjacent microdomains are 42 nm, 32 nm and 25 nm whereas the PEO cylinder diameters were 19.3 nm, 17 nm and 11 nm respectively. The intense spots in the FFT pattern shown in the insets of the AFM images (Figures 1a-c) confirms the hexagonal arrangement of PEO cylinders. The detailed mechanism of the microphase separation and ordering is described in our previous works.[16-17-38]

3.2. Preparation of Nanoporous polymer template. In order to incorporate inorganic material features into the PS-PEO nanopatterns, chemical degradation and/or modification of the PEO blocks, a process that leads to removal and densification of the PEO domains to produce nanopores is necessary.[13-16] This has been achieved by ultrasonication of the thin films in anhydrous ethanol for different periods of time depending on the morphology and feature size of the PEO blocks. As reported, [13-16] the ethanol treatment leads to removal of PEO blocks but a thin layer exists on top of the nanopores consists of crystalline PEO and trapped ethanol molecules. The structural periodicity and dimensions are essentially unchanged after ethanol treatment as revealed by SEM images in Fig. 2 and described by Scheme 1. The optimized ultrasonication times are 17 min, 15 min, 10 min and 20 min for S1, S2 and S3 dots and S1 fingerprints respectively. Presumably, the reduction in the optimum time as molecular weight decreases is related to reduce mass transport limitations at smaller dimensions. Note that the ethanol exposure had to be carefully optimized as longer exposures/higher temperatures resulted in surface roughness or structural degradation of the films. Following ethanol exposure, all the images showed an increment in the phase contrast without affecting the long range order (Figs. 2a-d). Further, the cylinder to cylinder spacings and the PEO cylinder diameters remained unchanged. No thickness change was observed as

measured by ellipsometry (Table 1). No deformation or discontinuity of the nanoporous template was observed. The polymer nanoporous template formed is monolayer and well adhered to the substrate surface as previously reported by us.[16-17]

3.3. Fabrication of inorganic oxides and metal nanostructure arrays.

3.3.1. NiO nanodots: dimensional control. As outlined above, in order to increase the etch contrast the activated templates can be used to create ordered oxide nanopatterned arrays by metal inclusion and subsequent UV/Ozone treatment. In contrast to our previous studies, the methodology has been extended to fabrication of friendly materials here and particularly metals.[14-17] Attempts were made to adapt this strategy to produce silicon nanowire arrays by use of different hard masks and to determine the best suitable mask to fabricate good quality Si patterns. The nanoporous polymer templates from S2 and S3 were utilized to form ordered nickel oxide (NiO) and nickel (Ni) nanodot arrays. Figs. 3a, inset and 3c represents the AFM and SEM images of the NiO nanodots prepared using the templates of S2 and S3 respectively using 1 wt% and 0.6 wt% precursor-ethanolic solutions. Note that the reduced solution concentration is consistent with the pore volume decrease for films of smaller molecular weight. The concentrations of the precursor-ethanolic solutions were adjusted to avoid overfilling of the nanopores. The film thicknesses after spin coating the metal precursors before and after the UV/Ozone treatment are summarized in Table 1. It is suggested that the hydrophobic nature of PS prevents metal ion inclusion into the PS component whilst selective inclusion into the porous template is favoured by a combination of capillary forces and the affinity of PEO with the ionic solution. Because the ethanol treatment etched most of the PEO blocks but a very thin crystalline PEO layer reside within the nanopores which assist the process of inclusion of the metal ions.[16] The process of inclusion is highly rapid and takes place in a few seconds during spin coating consistent with this principle.[38] Ordered large area nanodot arrays were realized with uniform size/shape

and their arrangement mimics that of the original BCP patterns. The reduction in solution concentration clearly reflects the pore volume decrease for the films of smaller molecular weight. The average diameters of the nanodots were 22 ± 3 nm, 16 ± 2 nm for S2 and S3 respectively. The average nanodot heights were between 6-8 nm as measured by ellipsometry. The density of the nanodots on the substrate is measured approximately 1.1 x 10^{11} and 6.7 x 10^{11} nanodots cm^{-2}. The TEM cross-section in the inset of Figure 3a also confirms the ordered arrangement and the dimension of the nanodots. The nanodots are well-adhered to the substrate and there is no deformation or delamination noticed. This methodology of creation of oxide nanodots array allows dimensional and spatial control over a large substrate area (Scheme 1).

3.3.2. Generation of Ni metal nanodots: dimensional control. Importantly, these NiO nanodots arrays could be utilized to create Ni metal nanodots without affecting their spatial arrangement. This demonstrates the physical and mechanical robustness of the developed nanostructures. The reduction process employed a high temperature of 800^0C under Ar/H_2 flowing atmosphere for 4 h. Figs. 3b, inset and 3d represents the AFM and SEM images of the Ni nanodots prepared using S2 and S3 respectively. Similarly ordered nanodot arrangement was realized for both the samples. A reduction in the diameter and height is noticed for both the samples because of high temperature densification and chemical reduction. The average measured diameters of the nanodots were 18 ± 3 nm, 13 ± 2 nm for S2 and S3 respectively. The average nanodot heights were between 5-7 nm as measured by ellipsometry whereas the areal density was unchanged.

3.3.3. ZnO nanodots: Morphology control. A similar strategy was utilized to fabricate Zinc oxide (ZnO) nanodots and nanowire arrays using S1 nanoporous hole and line templates. The SEM images in Figs. 3e and 3f represents the ZnO nanodots and nanowire arrays using 0.8 wt% and 1.5 wt% precursor-ethanolic solutions. Large area arrays were realized with uniform

size/shape and their arrangement mimics that of the original BCP patterns (Scheme 1). The diameters of the nanodots and nanowires were ~ 24 nm and 18 nm respectively. The ellipsometry measured heights of the nanodots and nanowires were ~ 9 nm and 7 nm respectively. The nanowires were continuous and no diameter variation is noticed throughout their entire length. It should be noted that the concentration of the precursor solution is critical and was carefully optimized to obtain isolated and continuous nanowires (see supporting information).

3.3.4. Compositional analysis by XPS. The chemical composition of the oxide and metal nanodot and nanowire assemblies was confirmed by high resolution Ni 2p and Zn 2p XPS spectra. In Fig. 4a, Ni $2p_{3/2}$ and Ni $2p_{1/2}$ spectrum is shown for the nanodots prepared with S2 annealed at a temperature of 800^0C. The Ni 2p core level spectrum consists of four peaks at 856/861.9 eV and 873.6/880.5 eV corresponding to the Ni $2p_{3/2}$ and Ni $2p_{1/2}$ signals attributed to Ni^{2+} as the major phase.[39] A typical XPS survey spectrum (not shown) of nickel oxide nanodots after annealing confirms the expected presence of Si, O, C and Ni. The C1s feature is relatively small and demonstrates effective removal of carbon species during processing. Its intensity is consistent with adventitious material formed by adsorption and other contamination during sample preparation. The Ni $2p_{3/2}$ core level spectrum for the metal nanodots prepared with S2 (Fig. 4b) after the reduction process consists of a main photopeak at 852.6 eV and an associated satellite peak at 858.9eV can be attributed to metallic Ni.[40] This confirms complete reduction of NiO to metallic Ni without affecting the lateral ordering for the nanodot arrays. Similar spectra were observed for the nanodots prepared with lower molecular weight BCP (S3). Fig. 4c presents the XPS Zn 2p core-level spectra of the zinc oxide nanowire arrays prepared with S1. The XPS Zn 2p spectra are simple spin-orbit doublets formed by the Zn $2p_{3/2}$ and Zn $2p_{1/2}$ electrons with binding energies of 1021.6 eV and 1044.7 eV respectively.[41] This can be attributed to Zn^{2+} oxidation states of ZnO.

3.4. Fabrication of Si nanowire arrays

3.4.1. NiO and Ni masks: dimension control. In order to create Si nanostructure arrays (Scheme 1(I)) on the substrate surface, the oxides and metallic nanopatterns were used as resistant masks in the ICP etch process. Note that the initial silica etch (prior to the silicon etch to pattern transfer) removes the exposed native silica layer on top of the substrate but not the areas directly below the mask. Thus, the uppermost face of the silicon nanofeatures has a layer of native oxide following mask. Figs. 5a-f shows SEM top-down and cross-sectional images of the Si features formed (including the oxide mask) for different etch times. Fig. 5a demonstrates a densely packed, uniform, ordered arrangement of vertically aligned Si nanowire arrays over large areas after 5 min Si etch with NiO mask for S2. The average height of the Si nanowires is around 150 nm. The higher magnification image in the inset of Fig. 5a shows the wires to be of uniform diameter (~ 20 nm) along their length and no shadowing effect of mask is observed. Further, smooth sidewalls are produced. Similar hexagonally arranged dense vertically aligned Si nanowire arrays of height ~100 nm were formed after 5 min Si etch with Ni mask for S2. The average diameter and spacing between the nanowires remained unchanged. Fig. 5c shows large area view of the pattern transferred substrate for S3 with NiO, which demonstrate this protocol is applicable to smaller dimensions. The nanowires with good sidewall profile with average diameter and height of 15 nm and 150 nm for 5 min Si etch time. Densely packed Si nanowire patterns of diameter and height ~ 12 nm and 100 nm respectively are realized for a 5 min Si etch for S3 with Ni mask. No surface roughening or pattern damage is seen with decreasing the diameter or increasing the height of the wires.

Note that the silica etch step did produce some lateral etching of features which decreases the diameter of the masks. Table 1 shows the feature diameter for the BCP pattern, the ‘activated’ pattern, after inclusion and formation of the hard mask and following the etch

treatment. In all cases the diameter of features reduced on pattern transfer. Since the wires do not change in diameter down their length, it can be concluded lateral etching was performed by the silica etch whist the more selective silicon etch had little effect on the mask. Thus, nickel oxide and nickel can act as highly effective hard masks in the ICP etching process.

3.4.2. ZnO mask: Morphology control. The applicability of ZnO as an etch mask for fabricating vertically and horizontally aligned nanowire patterns was also examined (Scheme 1). Fig. 5e shows large area dense vertically aligned nanowire arrays for 10 min Si etch with ZnO nanodots as an etch mask prepared using S1. The diameter and height of the nanowires were ~ 20 nm and 400 nm respectively. No sloping or tapering of the features is noticed. The higher magnification SEM image in the inset reveals nanowires with good sidewall profile and uniform diameter through their entire length. In few of the nanowires, nanoparticle-like deposition was observed towards the tip which might be because of the deposition of amorphous polymer layer during the etch process as explained before.[15] Fig. 5f shows the SEM images of densely packed, uniform, ordered arrangements of horizontal Si nanowires over large areas of the substrate for 3 min Si etch with ZnO mask formed by S1. The significant contrast enhancement suggests pattern transfer has occurred. A higher magnification image (inset of Figure 5f) demonstrate that the nanowires are continuous and of regular diameter (16 nm) along the length. The centre to centre nanowire spacing remained unchanged. This implies that the etching does not damage the original ‘mask’ to a significant extent.

3.4.3. Control over aspect ratio. Because of the hardmask character, the heights of the resultant vertically aligned nanowire patterns can be varied by changing the Si etch time without altering other processing conditions. At the longer etch times, well defined good quality nanowire arrays can be formed which reflects the etch resistant ability of the etch masks. Figs. 6a-e shows the cross-sectional SEM images of the hexagonal patterned uniform

Si nanopillars (or nanowires) with vertical smooth sidewalls of average heights about 50 nm, 100 nm, 250 nm, 400 nm and 500 nm for 2 min, 4 min, 8 min, 12 min and 15 min Si etch periods respectively with NiO as a resistant mask prepared with S2. All the images demonstrate good coverage of the nanopillar/nanowire arrays over a large area. The diameters of the nanopillars are almost equal throughout its entire length with little indication of narrowing or broadening. The images reveal quite narrow distribution of the aspect ratio of the wires. The higher magnification image shown in the inset of Fig. 6d reveals nanoparticle like deposition at the tip portion of the nanowires for longer etch times. The variation of average nanowire height with the Si etch time using NiO as a hard mask is plotted (Supporting Information) which increases linearly with etch time at a constant rate 33 nm min^{-1}. Similarly well ordered uniform Si nanopillars (or nanowires) with vertical smooth sidewalls of average heights about 40 nm, 80 nm, 160 nm, 250 nm and 320 nm for 2 min, 4 min, 8 min, 12 min and 15 min Si etch periods respectively with Ni as a resistant mask prepared with S2 as shown in the cross-sectional SEM images (Figs. 6f-j). Compared to the Si nanowires formed with NiO mask, better quality smooth sidewall profile without any surface roughness on the nanowires were realized using Ni as resistant mask. No surface pattern damage is seen with increasing the height of the nanowires. Thus, ultra dense, high aspect ratio vertical silicon nanopillars/wires with a controlled placement and spacings over a large area can be realised by using both NiO and Ni as hard mask in the ICP etching process. The average Si etch rate measured using Ni is around 22 nm min^{-1} (Supporting Information). This might be due to more erosion rate of the Ni mask than NiO but no significant diameter variation is noticed along the nanowire length. A well balanced etch/deposition process, gas flow rates was selected to avoid sidewall corrugation or scalloping and mask erosion. Further, low temperature was chosen to improve the silicon etching anisotropy and to decrease the etch rate of the masks.[15]

3.4.4. Quality of the nanowires by cross-sectional TEM and EDAX mapping. The morphology, interface, crystallinity of the vertically and horizontally aligned Si nanowire patterns as well as an estimation of the mask erosion rates (viz. NiO and ZnO) was further examined using TEM cross-sections. This is important because detailed assessment of the pattern transfer process is needed. Fig. 7a show micrographs of the well ordered equidistant array (~32 nm) of 5 min etched nanowires on Si substrates using NiO mask developed from S2. The higher magnification image (Fig. 7b) reveal Si nanowires of about 150 nm heights and 18-20 nm diameter with NiO masks on the upper surface. These data confirm the robustness of the mask in these etch conditions. The quality of the sidewalls was also revealed by the higher magnification TEM image. As can be seen, the diameter of the nanowires (~15 nm) remained unaltered along their length. The adhesion of the mask and its' mechanical integrity is also indicated by the robustness of the features during FIB processing. Elemental composition was confirmed by high resolution EDAX mapping and the distribution of Ni, O and Si are shown in Fig. 7c. The Si and Ni map shows a homogeneous distribution of silicon corresponding to each nanowire with sharp elemental interface with nickel oxide suggesting no inter-diffusion occurs after pattern transfer. The O map confirms the presence of oxides in nickel oxide at top and native silica layer of the substrate. Fig. 7d show the higher magnification image of the well ordered array (~32 nm) of 5 min etched nanowires on Si substrates with Ni at top for S2. The nanowires are of about 100 nm heights with Ni masks of diameter ~16 nm at top. The diameter of the Si nanowires of about 15 nm equal throughout their length. The Si and Ni map shows a homogeneous distribution of silicon corresponding to each nanowire with sharp elemental interface with nickel while O map confirms the formation of nickel metal at top and native silica layer of the substrate. This also suggests better masking ability for Ni mask than NiO.

Figs. 7f-h reveals the masking ability of horizontally aligned ZnO nanowire arrays to create Si nanowires prepared using S1. Fig. 7f shows hexagonally arranged ordered array of Si nanowires with ZnO at top. A clear contrast difference is noticed at the top of the nanowire due to ZnO which shows the mask was not removed through the pattern transfer process. The diameter and spacings of the nanowires remained unchanged which is 16 nm and 42 nm respectively. The higher magnification image (Fig. 7g) reveals small variation in diameter of the nanowires which decreases towards top of the wire. All of the wires investigated had smooth sidewalls. Elemental composition shown in Figure 7h reveals clear interface between Si, O and Zn. The measured thickness of the ZnO mask is around 6 nm reveals the effectiveness of the mask after the pattern transfer process.

Importantly, the HRTEM images for both the vertically and horizontally aligned nanowires (See Supporting Information) reveal highly crystalline structure with no sign of etch related amorphortization. The lattice fringes are continuous between bulk and nanowire silicon indicating no stacking or other defects and hence no re-crystallization during etching. The image shows the lattice fringes with spacing 3.11 Å across the wires agrees reasonably well with the Si FCC (111) interplanar distances.[42] The 54^0 angle of the (111) fringes with the substrate surface plane is consistent with the (100) orientation of the Si wafer. Thus, highly dense uniform 1D silicon nanowire arrays with controlled crystallographic orientation could be created through selective etching of the silicon wafers of chosen orientations.

4. Conclusion

Hexagonally arranged self-assembled PS-b-PEO nano dots/line patterns were realized by a simple solvent annealing process as a function of annealing temperature and annealing solvent/s. The dimension and lateral spacings can be controlled by the molecular weight of BCP. An effective ethanol treatment was followed for the modification of the PEO cylinders to create templates for the generation of inorganic materials without pattern damage. The

nickel oxide and zinc oxide nanodots and nanowire arrays were generated by selective metal ion inclusion and subsequent Uv/Ozone treatment which mimics the original self-assembled BCP pattern. Nickel metal was produced further by the reduction process of NiO under Ar/H_2 atmosphere at high temperature without any pattern damage. We demonstrate the pattern transfer ability and effectiveness of different etch masks to fabricate horizontally and vertically aligned uniform nanowire arrays over large substrate area with controlled placement and density. All of the masks were found to have the ability to form large area, identical ordered, crystalline, vertically and horizontally aligned Si nanowire arrays with a smooth sidewall profile through ICP Si etch process. Both lateral and longitudinal variation of the Si nanopatterns was achieved by varying the molecular weight of the BCP and the Si etch time. Compared to dimension and quality of the Si patterns formed, Ni metal shows better masking ability regarding uniform, smooth sidewall profile and less erosion speed. No additional defects or inter-diffusion of the materials was observed during the pattern transfer process. This self-assembled hardmask nanolithography can also be an important component in the manufacturing of nanoscale devices with high throughput and low cost compatible with current lithography.

Author information

Corresponding Authors

*Email: morrism2@tcd.ie; g_tandra@yahoo.co.in

Notes

The authors declare no competing financial interest.

Acknowledgements

We acknowledge financial support from the Science Foundation Ireland AMBER grant 12/RC/2278 and Semiconductor Research Corporation (SRC) grant 2013-OJ-2444. The

contribution of the Foundation's Principal Investigator support is also acknowledged. We would also like to thank Dr. Clive Downing for the TEM assistance.

REFERENCES

[1] Chan, C. K.; Peng, H. L.; Liu, G.; McIlwrath, K.; Zhang, X. F.; Huggins, R. A.; Cui, Y. High-performance lithium battery anodes using silicon nanowires. *Nat. Nanotechnol.* **2008,** *3*, 31-35.

[2] Goldberger, J.; Hochbaum, A. I.; Fan, R.; Yang, P. D. Silicon vertically integrated nanowire field effect transistors. *Nano Lett.* **2006,** *6*, 973-977.

[3] Trivedi, K.; Yuk, H.; Floresca, H. C.; Kim, M. J.; Hu, W. Quantum Confinement Induced Performance Enhancement in Sub-5-nm Lithographic Si Nanowire Transistors. *Nano Lett.* **2011,** *11*, 1412-1417.

[4] Moonen, P. F.; Yakimets, I.; Huskens, J. Fabrication of Transistors on Flexible Substrates: from Mass-Printing to High-Resolution Alternative Lithography Strategies. *Adv. Mater.* **2012,** *24*, 5526-5541.

[5] Doerk, G. S.; Cheng, J. Y.; Singh, G.; Rettner, C. T.; Pitera, J. W.; Balakrishnan, S.; Arellano, N.; Sanders, D. P. Enabling complex nanoscale pattern customization using directed self-assembly. *Nat. Commun.* **2014,** *5*.

[6] Cheng, J. Y.; Ross, C. A.; Chan, V. Z. H.; Thomas, E. L.; Lammertink, R. G. H.; Vancso, G. J. Formation of a cobalt magnetic dot array via block copolymer lithography. *Adv. Mater.* **2001,** *13*, 1174-+.

[7] Segalman, R. A.; Hexemer, A.; Hayward, R. C.; Kramer, E. J. Ordering and melting of block copolymer spherical domains in 2 and 3 dimensions. *Macromolecules* **2003,** *36*, 3272-3288.

[8] Cheng, J. Y.; Ross, C. A.; Thomas, E. L.; Smith, H. I.; Vancso, G. J. Fabrication of nanostructures with long-range order using block copolymer lithography. *Appl. Phys. Lett.* **2002,** *81*, 3657-3659.

[9] Lopes, W. A.; Jaeger, H. M. Hierarchical self-assembly of metal nanostructures on diblock copolymer scaffolds. *Nature* **2001,** *414*, 735-738.

[10] Ruiz, R.; Kang, H. M.; Detcheverry, F. A.; Dobisz, E.; Kercher, D. S.; Albrecht, T. R.; de Pablo, J. J.; Nealey, P. F. Density multiplication and improved lithography by directed block copolymer assembly. *Science* **2008,** *321*, 936-939.

[11] Borah, D.; Shaw, M. T.; Rasappa, S.; Farrell, R. A.; O'Mahony, C.; Faulkner, C. M.; Bosea, M.; Gleeson, P.; Holmes, J. D.; Morris, M. A. Plasma etch technologies for the development of ultra-small feature size transistor devices. *J. Phys. D-Appl. Phys.* **2011,** *44*, 174012.

[12] Farrell, R. A.; Kinahan, N. T.; Hansel, S.; Stuen, K. O.; Petkov, N.; Shaw, M. T.; West, L. E.; Djara, V.; Dunne, R. J.; Varona, O. G.; Gleeson, P. G.; Jung, S. J.; Kim, H. Y.; Kolesnik, M. M.; Lutz, T.; Murray, C. P.; Holmes, J. D.; Nealey, P. F.; Duesberg, G. S.; Krstic, V.; Morris, M. A. Large-scale parallel arrays of silicon nanowires via block copolymer directed self-assembly. *Nanoscale* **2012,** *4*, 3228-3236.

[13] Ghoshal, T.; Maity, T.; Godsell, J. F.; Roy, S.; Morris, M. A. Large Scale Monodisperse Hexagonal Arrays of Superparamagnetic Iron Oxides Nanodots: A Facile Block Copolymer Inclusion Method. *Adv. Mater.* **2012,** *24*, 2390-2397.

[14] Ghoshal, T.; Ntaras, C.; O'Connell, J.; Shaw, M. T.; Holmes, J. D.; Avgeropoulos, A.; Morris, M. A. Fabrication of ultra-dense sub-10 nm in-plane Si nanowire arrays by using a novel block copolymer method: optical properties. *Nanoscale* **2016,** *8*, 2177-2187.

[15] Ghoshal, T.; Senthamaraikannan, R.; Shaw, M. T.; Holmes, J. D.; Morris, M. A. “In situ” hard mask materials: a new methodology for creation of vertical silicon nanopillar and nanowire arrays. *Nanoscale* **2012,** *4*, 7743-7750.

[16] Ghoshal, T.; Senthamaraikannan, R.; Shaw, M. T.; Holmes, J. D.; Morris, M. A. Fabrication of Ordered, Large Scale, Horizontally-Aligned Si Nanowire Arrays Based on an In Situ Hard Mask Block Copolymer Approach. *Adv. Mater.* **2014,** *26*, 1207-1216.

[17] Ghoshal, T. M., T; Senthamaraikannan, R; Shaw, M; Carolan, P; Holmes, J; Roy, S; Morris, M Size and space controlled hexagonal arrays of superparamagnetic iron oxide nanodots: magnetic studies and application. *Scientific Reports* **2013,** *3*, 2772.

[18] Hawker, C. J.; Wooley, K. L. The convergence of synthetic organic and polymer chemistries. *Science* **2005,** *309*, 1200-1205.

[19] Kim, S. O.; Solak, H. H.; Stoykovich, M. P.; Ferrier, N. J.; de Pablo, J. J.; Nealey, P. F. Epitaxial self-assembly of block copolymers on lithographically defined nanopatterned substrates. *Nature* **2003,** *424*, 411-414.

[20] Segalman, R. A.; Yokoyama, H.; Kramer, E. J. Graphoepitaxy of spherical domain block copolymer films. *Adv. Mater.* **2001,** *13*, 1152-1155.

[21] Thurn-Albrecht, T.; Schotter, J.; Kastle, C. A.; Emley, N.; Shibauchi, T.; Krusin-Elbaum, L.; Guarini, K.; Black, C. T.; Tuominen, M. T.; Russell, T. P. Ultrahigh-density nanowire arrays grown in self-assembled diblock copolymer templates. *Science* **2000,** *290*, 2126-2129.

[22] Cheng, J. Y.; Mayes, A. M.; Ross, C. A. Nanostructure engineering by templated self-assembly of block copolymers. *Nat. Mater.* **2004,** *3*, 823-828.

[23] De Rosa, C.; Park, C.; Thomas, E. L.; Lotz, B. Microdomain patterns from directional eutectic solidification and epitaxy. *Nature* **2000,** *405*, 433-437.

[24] Park, C.; Yoon, J.; Thomas, E. L. Enabling nanotechnology with self assembled block copolymer patterns. *Polymer* **2003,** *44*, 6725-6760.

[25] Zhao, J. C.; Jiang, S. C.; Ji, X. L.; An, L. J.; Jiang, B. Z. Study of the time evolution of the surface morphology of thin asymmetric diblock copolymer films under solvent vapor. *Polymer* **2005,** *46*, 6513-6521.

[26] Mokarian-Tabari, P.; Collins, T. W.; Holmes, J. D.; Morris, M. A. Cyclical "Flipping" of Morphology in Block Copolymer Thin Films. *ACS Nano* **2011,** *5*, 4617-4623.

[27] Fasolka, M. J.; Mayes, A. M. Block copolymer thin films: Physics and applications. *Ann. Rev. Mater. Res.* **2001,** *31*, 323-355.

[28] Gu, X. D.; Liu, Z. W.; Gunkel, I.; Chourou, S. T.; Hong, S. W.; Olynick, D. L.; Russell, T. P. High Aspect Ratio Sub-15 nm Silicon Trenches From Block Copolymer Templates. *Adv. Mater.* **2012,** *24*, 5688-5694.

[29] Ruiz, R.; Sandstrom, R. L.; Black, C. T. Induced orientational order in symmetric diblock copolymer thin films. *Adv. Mater.* **2007,** *19*, 587-591.

[30] Xu, J.; Hong, S. W.; Gu, W. Y.; Lee, K. Y.; Kuo, D. S.; Xiao, S. G.; Russell, T. P. Fabrication of Silicon Oxide Nanodots with an Areal Density Beyond 1 Teradots Inch-2. *Adv. Mater.* **2011,** *23*, 5755-+.

[31] Fang, Q. L.; Li, X. D.; Tuan, A. P.; Perumal, J.; Kim, D. P. Direct pattern transfer using an inorganic polymer-derived silicate etch mask. *J. Mater. Chem.* **2011,** *21*, 4657-4662.

[32] Lim, K. M.; Gupta, S.; Ropp, C.; Waks, E. Development of metal etch mask by single layer lift-off for silicon nitride photonic crystals. *Microelectron. Eng.* **2011,** *88*, 994-998.

[33] Rangelow, I. W. Dry etching-based silicon micro-machining for MEMS. *Vacuum* **2001,** *62*, 279-291.

[34] Krishnamoorthy, S.; Manipaddy, K. K.; Yap, F. L. Wafer-Level Self-Organized Copolymer Templates for Nanolithography with Sub-50 nm Feature and Spatial Resolutions. *Adv. Funct. Mater.* **2011,** *21*, 1102-1112.

[35] Hsieh, H. Y.; Huang, S. H.; Liao, K. F.; Su, S. K.; Lai, C. H.; Chen, L. J. High-density ordered triangular Si nanopillars with sharp tips and varied slopes: one-step fabrication and excellent field emission properties. *Nanotechnology* **2007,** *18*, 505305.

[36] Sanders, D. P. Advances in Patterning Materials for 193 nm Immersion Lithography. *Chem. Rev.* **2010,** *110*, 321-360.

[37] Ito, T.; Okazaki, S. Pushing the limits of lithography. *Nature* **2000,** *406*, 1027-1031.

[38] Ghoshal, T.; Shaw, M. T.; Bolger, C. T.; Holmes, J. D.; Morris, M. A. A general method for controlled nanopatterning of oxide dots: a microphase separated block copolymer platform. *J. Mater. Chem.* **2012,** *22*, 12083-12089.

[39] Wang, X. Y.; Wu, W.; Chen, Z. L.; Wang, R. H. Bauxite-supported Transition Metal Oxides: Promising Low-temperature and SO2-tolerant Catalysts for Selective Catalytic Reduction of NOx. *Scientific Reports* **2015,** *5*.

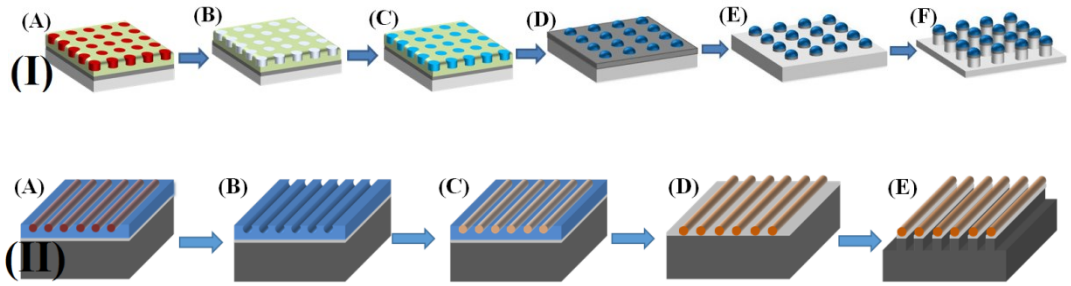
[40] Nesbitt, H. W.; Legrand, D.; Bancroft, G. M. Interpretation of Ni2p XPS spectra of Ni conductors and Ni insulators. *Phys. Chem. Miner.* **2000,** *27*, 357-366.

[41] Harati, M.; Love, D.; Lau, W. M.; Ding, Z. F. Preparation of crystalline zinc oxide films by one-step electrodeposition in Reline. *Mater. Lett.* **2012,** *89*, 339-342.

[42] Peng, K. Q.; Wu, Y.; Fang, H.; Zhong, X. Y.; Xu, Y.; Zhu, J. Uniform, axial-orientation alignment of one-dimensional single-crystal silicon nanostructure arrays. *Angew. Chem.-Int. Edit.* **2005,** *44*, 2737-2742.

Table 1. The film thicknesses and diameters of the PEO cylinders for the BCP before and after ethanol treatment, film thickness after spin coating precursor solutions, thickness and diameter of the nanopatterns before and after Uv/Ozone treatment and the diameter of the etched Si nanowires.

Mask	Polymer used	Film thickness/PEO cylinder diameter after solvent annealing (nm)	Film thickness/PEO cylinder diameter after ethanol treatment (nm)	Film thickness after spin coating precursor solution (nm)	Thickness/diameter of Nanopatterns after inclusion and Uv/Ozone treatment (nm)	Diameter of Si nanowires after pattern transfer (nm)
NiO	S2	25/17	25/17	~ 27	6-8/22 (nanodots)	20
NiO	S3	35/11	35/11	~ 36	6-8/16 (nanodots)	15
Ni	S2	25/17	25/17	-	5-7/18 (nanodots)	15
Ni	S3	35/11	35/11	-	5-7/13 (nanodots)	12
ZnO	S1	40/19.3	40/19.3	44	9/24 (nanodots)	20
ZnO	S1	40/19.3	40/19.3	42	7/18 (nanowires)	16



Scheme 1: Schematic illustration of the fabrication of vertical (I) and horizontal (II) ordered Si nanowires on substrate. (A) PEO cylinders (I) perpendicular and (II) parallel to the substrate in the PS matrix after solvent annealing (B) Modification of PEO cylinders creates nanoporous template (C) precursor solution spin coated on the template (D) metal oxide nanodots (I) and nanowires (II) formed after UV/ozone treatment (E and F) Si nanowires fabricated by consecutive silica and silicon ICP etch processes.

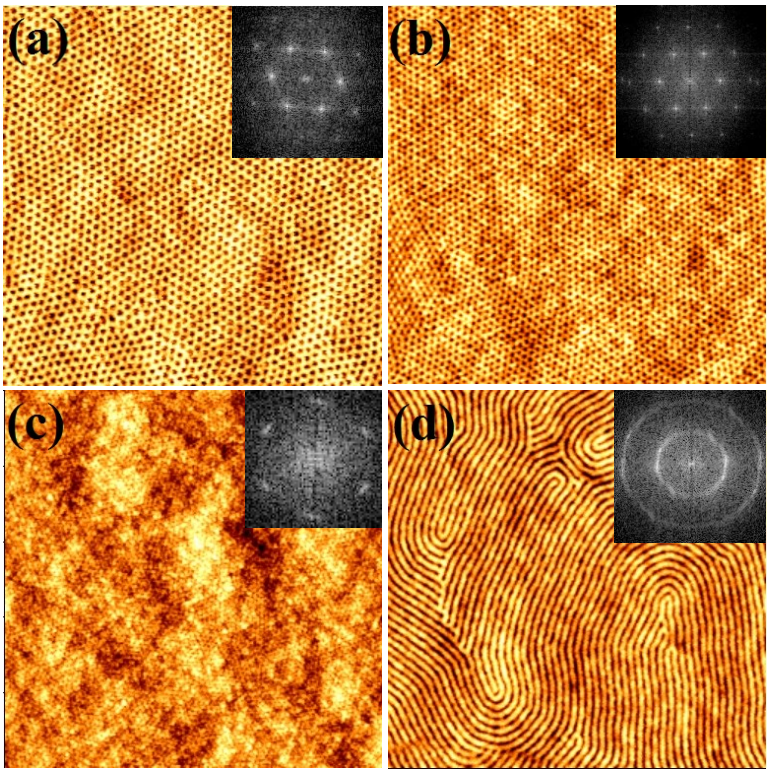


Figure 1 Tapping mode AFM images of the different molecular weight PS-PEO thin films solvent annealed for 1h (a) 42k-11.5k (S1) in toluene/water at 50^0 C, (b) 32k-11k (S2) in toluene at 50^0 C, (c) 16k-5k (S3) in toluene/water at 50^0 C and (d) 42k-11.5k (S1) in toluene at 60^0 C. All the images are 2 x 2 μm. Insets show corresponding FFT patterns.

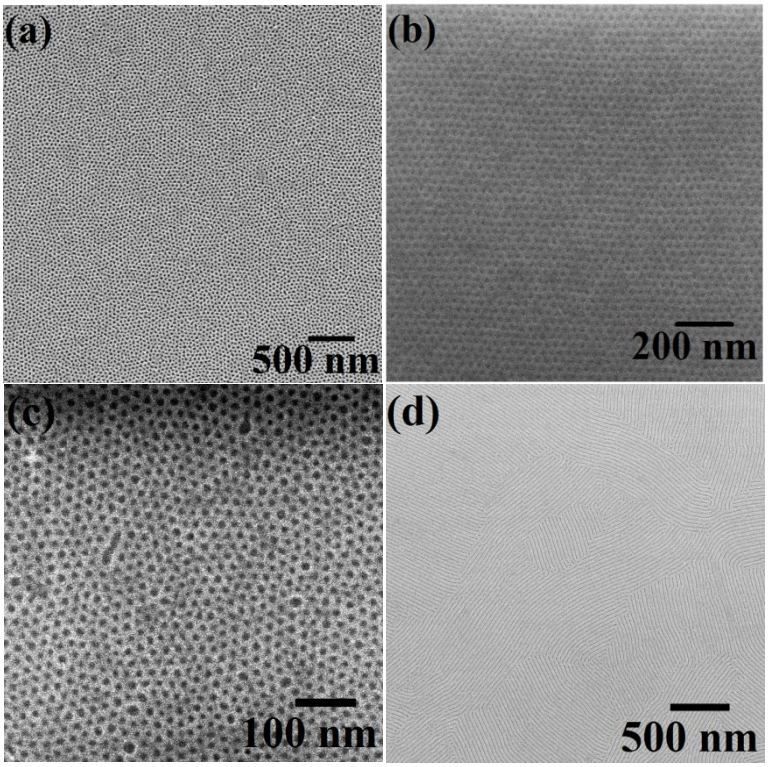


Figure 2 SEM images of the nanoporous templates after ultrasonication in anhydrous ethanol for different time (a) S1, 17 min, (b) S2, 15 min, (c) S3, 15 min and (d) S1, 20 min respectively.

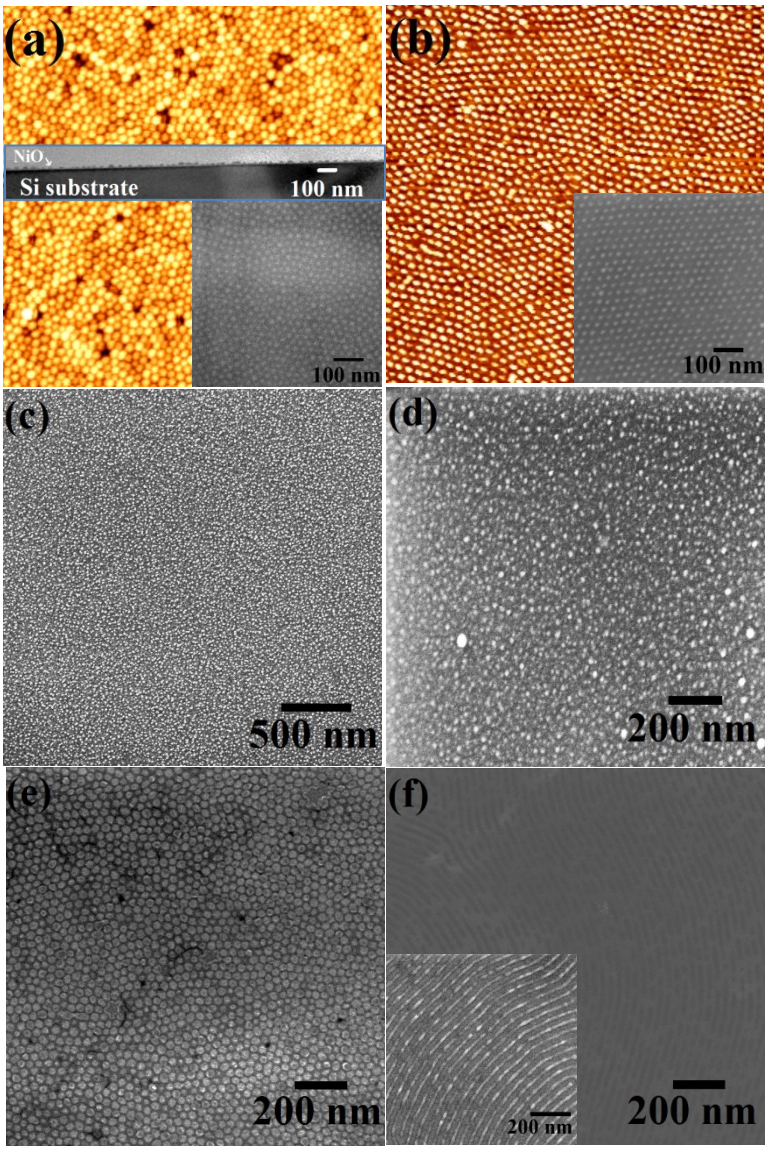


Figure 3 Well ordered nanodots patterns prepared by spin coating different precursor-ethanolic solution formed after UV/Ozone treatment (a) S2, NiO, (c) S3, NiO, (e) S1, ZnO. Ni metal nanodots patterns formed by reducing NiO at a high temperature of 800^0C under Ar/H_2 flowing atmosphere for 4 h for (b) S2 and (d) S3. (f) Horizontally aligned ZnO nanowire patterns by S1. Inset of (a) shows cross-sectional TEM image of well ordered NiO nanodots on Si substrate.

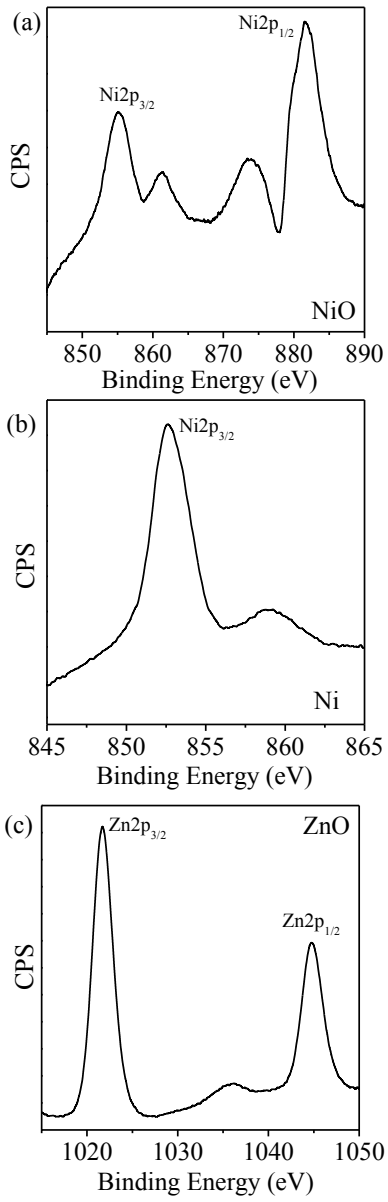


Figure 4 Ni 2p and Zn 2p spectra nanodots and nanowires for (a) NiO by S2, (a) Ni by S2 and (b) ZnO by S1 respectively.

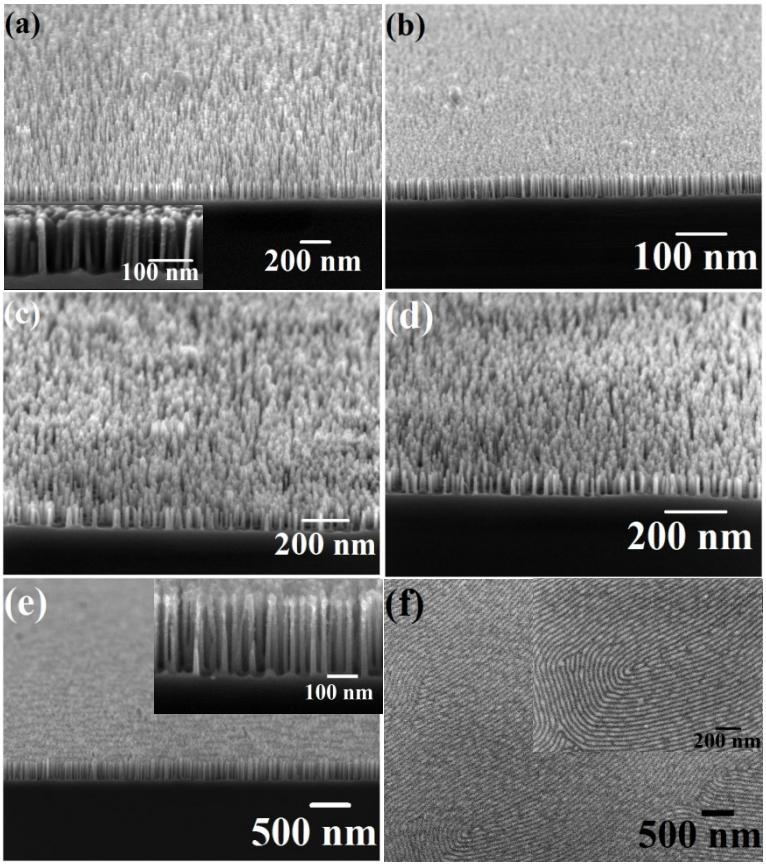


Figure 5 Vertically aligned Si nanowire patterns formed after silica and silicon etch for different Si etch time with different molecular weight PS-PEO system and different masking materials. (a) S2, NiO, 5 min, (b) S2, Ni, 5 min, (c) S3, NiO, 5 min, (d) S3, Ni, 5 min, (e) S1, ZnO, 10 min respectively. (f) Horizontally aligned Si nanowire patterns formed for S1 with ZnO after 3 min Si etch.

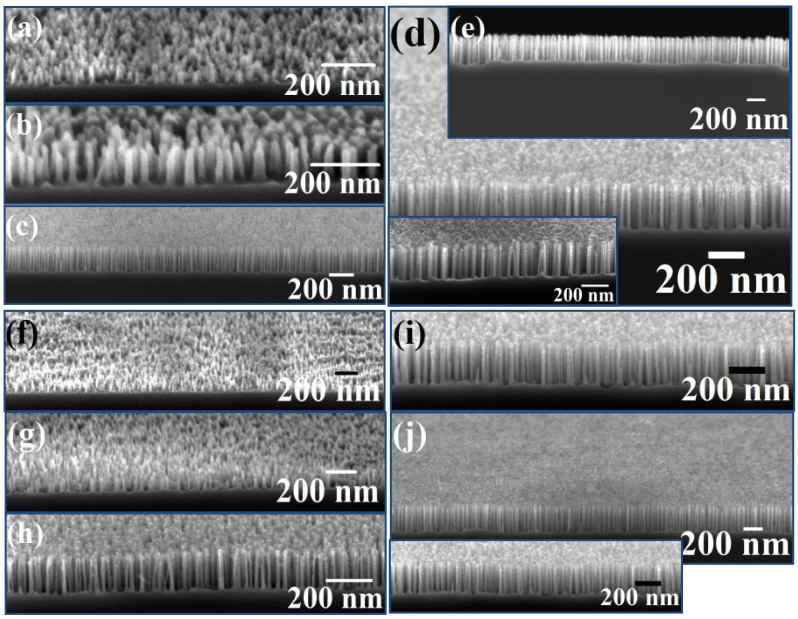


Figure 6 Vertically aligned Si nanowire patterns of different heights formed after silica and silicon etch for different Si etch time with different molecular weight PS-PEO system and different masking materials. (a-e) S2, NiO, 2 min, 4 min, 8 min, 12 min, 15 min, (f-j) S2, Ni, 2 min, 4 min, 8 min, 12 min, 15 min respectively.

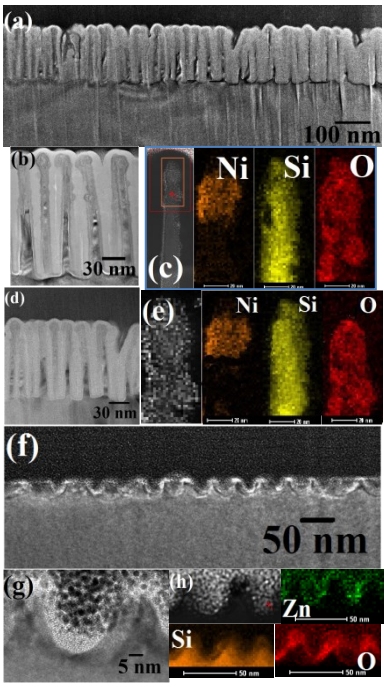


Figure 7 Cross-sectional TEM images of vertically and horizontally aligned nanowires with different etch mask for different Si etch time with (a, b) S2, NiO, 5 min (d) S2, Ni, 5 min, (f, g) S1, ZnO, 3 min respectively. (c), (e) and (h) represents corresponding elemental mapping for Ni, O, Si and Zn.